

Double Gravitational Wave Mergers

Johan Samsing^{1,2*}, Teva Ilan¹

¹*Department of Astrophysical Sciences, Princeton University, Peyton Hall, 4 Ivy Lane, Princeton, NJ 08544, USA*

²*Einstein Fellow*

Accepted XXX. Received YYY; in original form ZZZ

ABSTRACT

In this paper we study the dynamical outcome in which black hole (BH) binary-single interactions lead to two successive gravitational wave (GW) mergers; a scenario we refer to as a ‘double GW merger’. The first GW merger happens during the three-body interaction through a two-body GW capture, where the second GW merger is between the BH formed in the first GW merger and the remaining bound single BH. We estimate the probability for observing both GW mergers, and for observing only the second merger that we refer to as a ‘prompt second-generation (2G) merger’. We find that the probability for observing both GW mergers is only notable for co-planar interactions with low GW kicks ($\lesssim 10^1 - 10^2 \text{ kms}^{-1}$), which suggests that double GW mergers can be used to probe environments facilitating such interactions. For isotropic encounters, such as the one found in globular clusters, the probability for prompt 2G mergers to form is only at the percent level, suggesting that second-generation mergers are most likely to be between BHs which have swapped partners at least once.

Key words: gravitation – gravitational waves – stars: black holes – stars: kinematics and dynamics

1 INTRODUCTION

The recent gravitational wave (GW) detections by the Laser Interferometer Gravitational-Wave Observatory (LIGO) of binary black hole (BBH) mergers (Abbott et al. 2016b,c,a, 2017a,b), have initiated a wide range of studies on how such BBHs form and merge in our Universe (see Abbott et al. 2016d, and references therein). The merger channels that have been suggested to contribute include stellar clusters (Portegies Zwart & McMillan 2000; Banerjee et al. 2010; Tanikawa 2013; Bae et al. 2014; Rodriguez et al. 2015, 2016a,b,b; Askar et al. 2017; Park et al. 2017), primordial black holes (Bird et al. 2016; Cholis et al. 2016; Sasaki et al. 2016; Carr et al. 2016), active galactic nuclei discs (Bartos et al. 2017; Stone et al. 2017; McKernan et al. 2017), galactic nuclei (O’Leary et al. 2009; Hong & Lee 2015; VanLandingham et al. 2016; Antonini & Rasio 2016; Hoang et al. 2017), isolated field binaries (Dominik et al. 2012, 2013, 2015; Belczynski et al. 2016b,a), and field triples (e.g. Silsbee & Tremaine 2017; Rodriguez & Antonini 2018).

Theoretical work indicates that these channels likely result in similar merger rates and chirp mass distributions (e.g. Zevin et al. 2017), which has led to several discussions on how to observationally distinguish them. From this, it seems that the spins of the BHs and their orbital ec-

centricity in the LIGO band, are very promising parameters. Regarding spins, BH spins are naturally believed to be isotropically distributed for the dynamical channel (e.g. Rodriguez et al. 2016c; Farr et al. 2017), whereas the field binary channel is more likely to result in BH spins that are preferentially aligned (Kalogera 2000). In case of eccentricity, BBH mergers from the field binary channel are expected to be near circular at the time of observation (e.g. Voss & Tauris 2003), whereas a notable fraction of the dynamically assembled BBH mergers are likely to be eccentric in the LIGO band as a result of chaotic exchanges of angular momentum during their formation (e.g. Gültekin et al. 2006; Samsing et al. 2014; Antonini et al. 2016; Samsing et al. 2017; Samsing & Ramirez-Ruiz 2017; Samsing 2017; Samsing et al. 2018).

In this paper we study the role of post-Newtonian (PN) effects (e.g. Blanchet 2006) – or GR corrections – in few-body interactions, for exploring the interesting and distinct outcome in which a binary-single interaction results in not only one, but in *two* GW mergers; an outcome first studied numerically by Campanelli et al. (2008), and later dynamically by Samsing & Ilan (2018). To shorten the descriptions, we denote this outcome a *double GW merger*. In this scenario, the first GW merger forms through a standard two-body GW capture (e.g. Hansen 1972; Bae et al. 2017), while the three BHs temporary constitute a bound state (e.g. Samsing et al. 2014). After this follows the formation

* E-mail: jsamsing@gmail.com

of the second GW merger, which is between the BH formed in the first GW merger and the remaining bound BH. The endstate of the double GW merger scenario is therefore a single BH with a mass approximately that of the three initial BHs, and a velocity composed of the initial three-body center-of-mass (COM) velocity and any acquired GW kick velocity. We note here that this multi GW merger scenario is somewhat the GR equivalent of the classical multi stellar collision scenario described in, e.g., Fregeau et al. (2004).

In the work presented here, we explore two unique observables related to the double GW merger scenario: i) The first is the observation of both GW mergers, which naturally requires that the time between the first and the second GW merger, denoted t_{12} , is less than the observation time window ($< \mathcal{O}(10^1)$ years). For this outcome, we find that near co-planar interactions generally give rise to the shortest time interval t_{12} , which in a few cases is $< \mathcal{O}(\text{years})$. The reason for a co-planar preference is that in this case the angular momentum carried by the incoming single can significantly reduce the angular momentum of the initial target binary and thereby the GW life time. This makes the double GW merger channel an indirect probe of environments facilitating co-planar interactions. Although speculative, such environments may include rotationally supported systems, such as an active galactic nuclei (AGN) disk (e.g. Bellovary et al. 2016; Stone et al. 2017; Bartos et al. 2017; McKernan et al. 2017; Leigh et al. 2018). Another example is the class of disk-like systems forming in galactic nuclei as a result of vector resonant relaxation (e.g. Kocsis & Tremaine 2011, 2015; Roupas et al. 2017). ii) The second is the observation of only the second GW merger, which we in short will refer to as prompt second-generation (2G) merger. As most binary-single interactions are expected to be between objects of similar mass (Rodriguez et al. 2016a; Samsing & Ramirez-Ruiz 2017), prompt 2G mergers will most often be between two BHs with mass ratio about 1 : 2, where the heavier BH spins at ~ 0.7 . Recent studies have suggested that dynamical environments indirectly can be probed by the search for second-generation mergers (e.g. Antonini & Rasio 2016; Gerosa & Berti 2017; Rodriguez et al. 2018); however, the contribution from our presented prompt 2G channel has not been discussed in the literature so far. For a 2G merger to occur the time span t_{12} has to be smaller than the average encounter time scale for the considered dynamical system ($< 10^8$ years). In this case we also find that near co-planar interactions can significantly contribute to a prompt 2G population, whereas the rate of prompt 2G mergers in isotropic systems is suppressed.

The paper is structured as follows. In Section 2 we describe some of the basic properties related to binary-single interactions with and without GR corrections. This includes a definition of the relevant binary-single outcomes, and a description of how these distribute in orbital phase space. In Section 3 we present our main results on the formation of double GW mergers. We summarize our findings in Section 4.

2 BLACK HOLE BINARY-SINGLE INTERACTIONS

The initial total energy of a binary-single interaction broadly determines the range of possible outcomes and associated observables (e.g. Heggie 1975; Hut & Bahcall 1983; Samsing et al. 2014). If the total energy is positive, also known as the soft-binary (SB) limit, the interaction is always prompt, and will most likely lead to either an *ionization*, a *fly-by*, or an *exchange* endstate (e.g. Hut & Bahcall 1983; Hut 1983b). If the total energy is instead negative, also known as the hard-binary (HB) limit, the system can enter a bound state with a lifetime that generally is in the range of a few to several thousand initial orbital times (e.g. Hut & Bahcall 1983; Hut 1993). Such bound states often undergo highly chaotic evolutions under which two of the three objects have a relative high chance of merging (e.g. Fregeau et al. 2004; Samsing et al. 2014, 2017; Samsing & Ramirez-Ruiz 2017). This makes the HB limit interesting and highly relevant for the assembly of BBH mergers observable by LIGO (e.g. Gültekin et al. 2006; Samsing et al. 2014; Rodriguez et al. 2016a; Samsing & Ramirez-Ruiz 2017). We will in this paper therefore solely focus on the dynamics and outcomes of the HB limit.

2.1 Hard-Binary Interactions

A HB interaction either undergoes a direct interaction (DI) or a resonant interaction (RI), depending on the exact ICs (e.g. Hut & Bahcall 1983; Samsing et al. 2014; Samsing & Ilan 2018). These two interaction types are briefly discussed below, together with their relation to finite size effects and GR corrections.

A DI is characterized by having a relative short interaction time. The associated kinematics are generally such that after the single enters the binary, it directly pairs up with one of the members by ejecting the remaining member to infinity through a classical sling-shot maneuver (e.g. Samsing & Ilan 2018). Due to the short nature of this interaction type, finite sizes and GR effects rarely play a role here (e.g. Samsing et al. 2014).

A RI is by contrast characterized by having a long interaction time, as the three objects in this case enter a temporary bound state. The associated evolution of this state is often highly chaotic (e.g. Hut & Bahcall 1983; Samsing et al. 2014), which makes it possible for the system to enter a configuration where dissipative effects, such as GW emission and tides, become important for the subsequent dynamics (Samsing et al. 2017). To understand how, it was illustrated in, e.g., Samsing et al. (2014, 2017, 2018) that a typical RI can be described as a series of intermediate states (IMs) characterized by a binary, referred to as the IMS binary, with a bound single. Between each IMS the three objects undergo a strong interaction where they semi-randomly exchange energy and angular momentum. Each IMS binary is therefore formed with orbital parameters that are different from that of the initial target binary, which makes it possible for highly eccentric IMS binaries to form during the interaction. It is primarily during the evolution of these highly eccentric IMS binaries that GW emission can drain a notable amount of orbital energy and angular momentum out

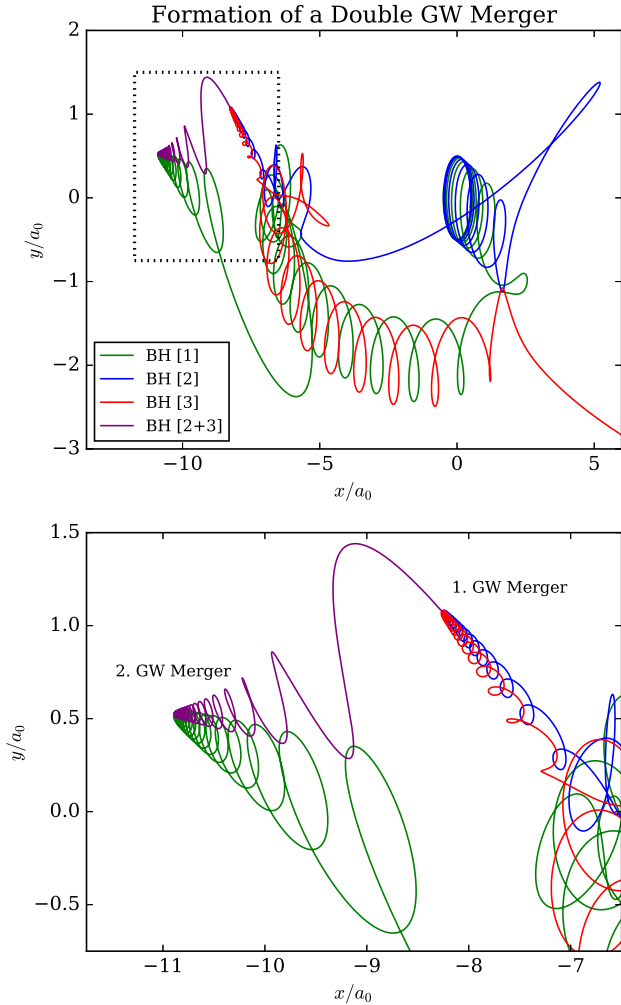


Figure 1. Dynamical formation of a double GW merger. *Top:* Orbital trajectories from an equal mass co-planar interaction between a BH binary and an incoming single BH, evolved using our N -body code that includes GW emission in the EOM at the 2.5PN level (Samsing et al. 2017). Each of the three BHs has a mass of $20M_{\odot}$, and the initial SMA is set to the low value of 10^{-4} AU for illustrative purposes. *Bottom:* Zoom in on the orbital parts showing the first GW merger (labeled ‘1. GW Merger’), and the second GW merger (labeled ‘2. GW Merger’). The zoom box is shown in the top plot by a dotted box. As seen, the first GW merger happens here between BH[2] and BH[3] as a result of a highly eccentric GW capture (e.g. Samsing et al. 2014), from which a new BH, denoted by BH[2+3], is formed. This first GW merger happens while the three BHs are still bound to each other, which implies that BH[2+3] and the remaining single BH[1] are also bound to each other after the formation of BH[2+3] – given the GW kick velocity of BH[2+3] is negligible. In that limit, the system now undergoes its second GW merger, which is between BH[2+3] and BH[1]. For the simulation results shown here, we have for simplicity assumed that the GW kick velocity of BH[2+3] is zero, and the mass of BH[2+3] is the mass of BH[1] plus the mass of BH[2]. As described in Section 3.3.1, the time span from first to second GW merger takes its shortest values for binary-single interactions where the total angular momentum is close to zero, a scenario that is only possible in near co-planar interactions. An observed population of double GW mergers will therefore be an indirect probe of environments facilitating near co-planar binary-single interactions, such as disk-like environments.

of the three-body system. The change in outcome distributions from including GW emission in the EOM, is therefore linked to the formation of highly eccentric IMS binaries in RIs. This will be described further below.

2.2 Outcomes and Endstates

In the classical case where the objects are assumed point-like and only Newtonian gravity is included in the N -body EOM, the only possible endstate in the HB limit is a binary with an unbound single (e.g. Heggie 1975; Hut & Bahcall 1983). We refer to this endstate binary as the post-interaction binary in analogy with Samsing & Ramirez-Ruiz (2017); Samsing et al. (2018). In this notation, if the initial incoming single is a member of the post-interaction binary the endstate will be an exchange.

If one includes finite sizes, a collision between any two of the three objects become a possible endstate. Such collisions predominately form in RIs, as a result of an IMS binary forming with a pericenter distance that is smaller than the sum of the radii of the two IMS binary members (e.g. Fregeau et al. 2004; Samsing et al. 2017). The probability for a post-interaction binary to undergo a collision is in comparison relatively small, as each binary-single interaction leads to several IMS binaries compared to only one post-interaction binary. As a result, the majority of the collisional products forming in binary-single interactions will therefore have the remaining single as bound companion. As argued in Samsing et al. (2017), collisions contribute significantly to the merger rate when the interacting objects are solar type objects, and less if they are compact, such as a white-dwarf, a neutron-star (NS) or a BH. In the latter case, dissipative captures (tides and GWs) greatly dominate over collisions (Samsing et al. 2018).

If GW emission is included in the EOM (in our simulations through the 2.5PN term), a close passage between any two of the three objects can lead to a significant loss of orbital energy and angular momentum (e.g. Gültekin et al. 2006). If the energy loss is large enough, the two objects will undergo a GW capture with a merger to follow, which we in the three-body case refer to as a *GW inspiral* in analogy with Samsing et al. (2014). This GW inspiral scenario most often happens between IMS binary members, as these have a finite probability for being formed with a high eccentricity and thereby small pericenter distance, as described in Section 2.1. As demonstrated by Samsing et al. (2014), the probability for forming a GW inspiral can therefore be estimated from simply deriving the fraction of IMS binaries that form with a GW inspiral time that is shorter than the orbital time of the bound single. As this GW inspiral time has to be comparable to the orbital time of the initial binary, the IMS binary eccentricity must be close to unity, which explains why the binary-single channel is a natural producer of high eccentricity BBH mergers (Samsing & Ramirez-Ruiz 2017; Samsing 2017).

Figure 1 shows an example of a GW inspiral forming during a binary-single interaction. As for the collisions, in the limit where GW velocity kicks are negligible, the merger remnant formed as a result of the GW inspiral will still be bound to the remaining single after its formation. This final binary, now composed of the single and the merger product, will undergo its own GW merger on a timescale that depends

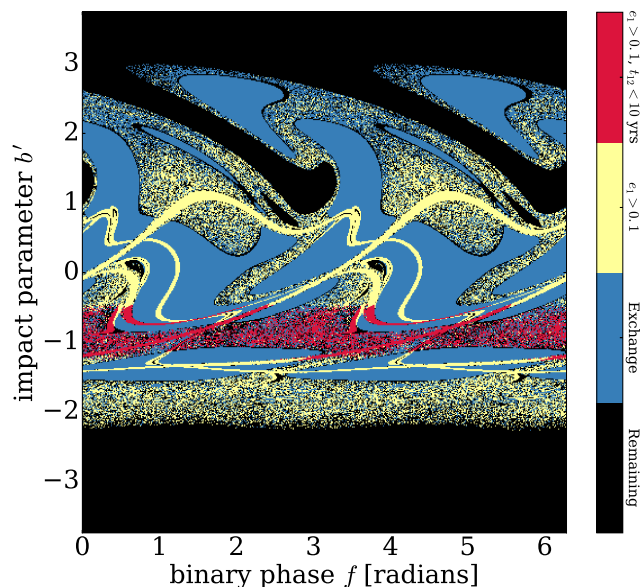


Figure 2. Endstate topology. Distribution of binary-single endstates, as a function of the binary phase f , measured at the time the single is exactly $20 \times a_0$ away from the binary COM, and the rescaled impact parameter $b' = (b/a_0)(v_\infty/v_c)$ (see Section 3.2). We refer to this endstate distribution as the endstate topology. The shown distribution is derived from equal mass co-planar binary-single BH interactions ($\gamma = 0$), where each BH has a mass of $20M_\odot$, and the SMA of the initial target binary is $a_0 = 10^{-2}$ AU. *Blue*: All interactions resulting in a classical exchange interaction. *Yellow*: Interactions that result in a merging BH binary that has an orbital eccentricity $e_1 > 0.1$ when its GW peak frequency is at 50 Hz. This is the population that is likely to appear eccentric when observed by an instrument similar to LIGO. *Red*: Interactions from the yellow population ($e_1 > 0.1$ at 50 Hz) that further have a timespan from first to second GW merger $t_{12} < 10$ years. We have here assumed a GW kick velocity of $v_K = 0$. *Black*: All remaining endstates and unfinished interactions. How the fraction of the potential observable red population ($e_1 > 0.1$ at 50 Hz with $t_{12} < 10$ years) scales with the initial SMA a_0 and the GW kick velocity v_K , is shown in Figure 5 and discussed in Section 3.

sensitively on the ICs, as will be described in Section 3. It is the inspiral time of this second GW merger that ultimately determines if the double GW merger scenario is observable or not.

2.3 Distribution of Endstates

To understand which binary-single ICs lead to exchanges, collisions, single and double GW mergers, we now consider a mapping we refer to as the endstate topology (Hut 1983a; Samsing & Ilan 2018). This topological mapping refers to the graphical representation of the distribution of endstates, as a function of the initial binary phase f and impact parameter b , as further described in Figure 2 and 3, and Hut (1983a); Samsing & Ilan (2018). We note here that for isotropic encounters each point in the f, b space is equally likely.

The endstate topology derived for a co-planar equal mass BH binary-single interaction is shown in Figure 2, where *blue* denotes an exchange endstate, *yellow* all endstates for which the endstate binary (that eventually merges

due to GW emission) has an eccentricity $e_1 > 0.1$ when its GW peak frequency $f_{1\text{GW}}$ is at 50 Hz, and *black* all remaining endstates and unfinished interactions (the *red* relates to double GW mergers and will be explained in Section 3.2). For calculating the eccentricity distribution at 50 Hz, we evolved the endstate binary in question using the quadrupole formalism from Peters (1964), together with $f_{1\text{GW}}$ using the approximation presented in Wen (2003). We note that the vast majority of the highly eccentric GW inspiral mergers originate from IMS binaries undergoing either a GW inspiral or a direct collision.

As seen in Figure 2, the distribution of endstates is far from random, despite the chaotic nature of the three-body problem (e.g. Hut 1983a; Samsing & Ilan 2018). Generally, the large-scale wave-like pattern arises from the distribution of how much energy the single ejected during the first sling-shot maneuver receives (see Section 2.1), as the homogenous regions (neighboring f, b points have the same endstate) arise from DIs and the random regions (neighboring f, b points have semi-random endstates) arise from RIs (e.g. Samsing & Ilan 2018). The asymmetry along the b -axis relates to which way the binary rotates relative to the incoming single, where $b > 0$ corresponds to prograde motion, and $b < 0$ to retrograde motion. Also, the initial total angular momentum, L_0 , changes along the b -axis, as the angular momentum brought in by the single is $\propto b$. As discussed in the sections below, understanding how L_0 distributes is the key to understand what ICs that will lead to double GW mergers with a time space t_{12} short enough for either resulting in two observable mergers, or a single prompt 2G merger.

3 FORMATION OF DOUBLE GW MERGERS

Having provided an understanding of binary-single interactions with GR and finite size effects, we are now in a position to study our proposed double GW merger scenario. We proceed below by first describing the dynamics leading to the two GW mergers (Section 3.1 and 3.2), after which we discuss the prospects for observing either both GW mergers (Section 3.3), or just the second prompt 2G merger (Section 3.4). For this, we use analytical relations together with full numerical 2.5PN simulations including GW kicks. We note here that at least one of the two GW mergers is likely to have a notable eccentricity when entering the LIGO band, observing double GW mergers therefore heavily relies on the development of accurate eccentric GW templates (e.g. Harry et al. 2016; Huerta et al. 2017; Gondán et al. 2017; Huerta et al. 2018).

3.1 First GW Merger

The first GW merger forms through a GW inspiral, while the three objects are still bound to each other, as described in Section 2.2. The resultant BH has a mass close to the total mass of the two merging BHs (ignoring relativistic mass loss), and a velocity that is composed of the initial COM velocity of the two merging BHs, and a GW kick velocity gained through asymmetric GW emission at merger (e.g. Baker et al. 2006; González et al. 2007; Lehner & Pretorius 2014). The magnitude of the GW kick velocity depends on

the relative BH spins and masses, and can easily reach values of order $\sim 10^2 - 10^3 \text{ km s}^{-1}$ (e.g. Centrella et al. 2010). The GW kick velocity can therefore significantly affect the dynamics leading to the second GW merger, and plays as a result an important role. We study the effect from GW velocity kicks in Section 3.3.2 (co-planar case) and Section 3.3.3 (isotropic case). As the first GW merger generally enters the LIGO band with a notable eccentricity (Samsing et al. 2014; Samsing & Ramirez-Ruiz 2017), an observation of an eccentric BBH merger is therefore the best indication of a potential double GW merger.

3.2 Second GW Merger

The second GW merger forms through an inspiral between the remaining bound single BH and the BH formed in the first GW merger. We refer in the following to these two BHs as BH₁ and BH₂, respectively. The SMA, a_{12} , and eccentricity, e_{12} , of this [BH₁, BH₂] binary measured just after the formation of BH₂, can be written by the use of standard classical mechanics as,

$$a_{12} = \left[\frac{2}{|\mathbf{R}_{12}|} - \frac{(\mathbf{v}_{12} + \mathbf{v}_K)^2}{3Gm_{\text{BH}}} \right]^{-1}, \quad (1)$$

$$e_{12} = \left[1 - \frac{3}{4} \frac{|\mathbf{L}_{12} + \mathbf{L}_K|^2}{Gm_{\text{BH}}^3 a_{12}} \right]^{1/2}, \quad (2)$$

where m_{BH} is the mass of one of the three initial (equal mass) BHs, \mathbf{v}_K is the GW velocity kick vector in the frame of BH₂, \mathbf{R}_{12} and \mathbf{v}_{12} are the position and velocity vectors of BH₂ in the frame of BH₁ assuming $\mathbf{v}_K = 0$, and \mathbf{L}_{12} and \mathbf{L}_K are the angular momentum vectors $(2m_{\text{BH}}/3)\mathbf{R}_{12} \times \mathbf{v}_{12}$, $(2m_{\text{BH}}/3)\mathbf{R}_{12} \times \mathbf{v}_K$, respectively. We have in these expressions assumed for simplicity that the mass of BH₂ is $= 2m_{\text{BH}}$, although the actual mass will be a few percent lower due to relativistic mass loss at merger (e.g. Lehner & Pretorius 2014). An illustration of the orbital configuration right after the formation of BH₂ is shown in Figure 4.

Using the above relations for a_{12} and e_{12} , one finds that the corresponding pericenter distance $r_{12} = a_{12}(1 - e_{12})$, in the high eccentricity limit, can be written as,

$$r_{12} \approx \frac{3}{8} \frac{|\mathbf{L}_{12} + \mathbf{L}_K|^2}{Gm_{\text{BH}}^3}. \quad (3)$$

While \mathbf{R}_{12} , \mathbf{v}_{12} , and \mathbf{v}_K depend sensitively on the ICs, we find that the initial total three-body angular momentum, denoted $\mathbf{L}_0 = \mathbf{L}_B + \mathbf{L}_S$, where \mathbf{L}_B and \mathbf{L}_S are the angular momentum vectors of the initial binary and the incoming single, respectively (See Figure 3), do not change significantly during the interaction. This follows from that the first GW inspiral generally forms on a low angular momentum orbit, meaning that only a small amount of angular momentum is emitted in the first GW merger. As a result, one can write \mathbf{L}_{12}^2 to leading order as,

$$\mathbf{L}_{12}^2 \approx \mathbf{L}_0^2 = \frac{Gm_{\text{BH}}^3 a_0}{2} \left[1 + \frac{4}{3} b'^2 + \frac{4}{\sqrt{3}} b' \cos(\gamma) \right], \quad (4)$$

where a_0 is the SMA of the initial circular target binary, γ is the smallest angle between \mathbf{L}_B and \mathbf{L}_S (See Figure 3),

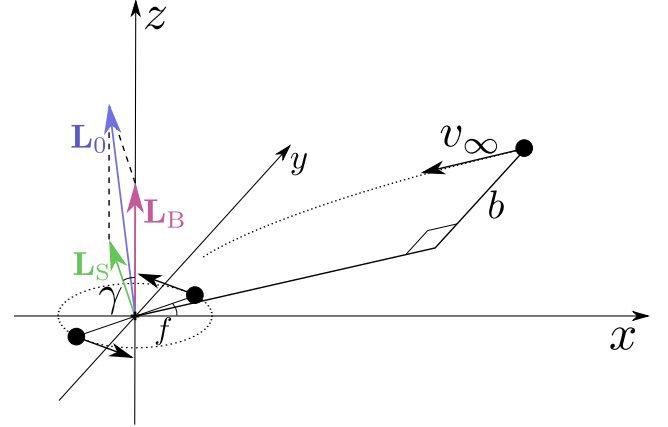


Figure 3. Illustration of the binary-single ICs. The three large black dots represent the interacting BHs, two of which initially are in a binary that here is centered at $(0, 0, 0)$. The impact parameter b and relative velocity v_∞ are both defined at infinity, where f refers to the binary phase at the time the single is exactly $20 \times a_0$ away from the binary COM (Samsing & Ilan 2018). The initial angular momentum vectors of the binary and the single, respectively, are here denoted by \mathbf{L}_B (purple) and \mathbf{L}_S (green), where their sum is labeled by $\mathbf{L}_0 = \mathbf{L}_B + \mathbf{L}_S$ (blue). The smallest angle between \mathbf{L}_B and \mathbf{L}_S is denoted by γ , and a co-planar interaction therefore has $\gamma = 0$. As indicated by the velocity arrows, the binary is initially set to rotate counter-clockwise, which implies that $\mathbf{L}_B \cdot \mathbf{L}_S > 0$ for $b > 0$, and vice versa. From this follows that if $b < 0$, then $|\mathbf{L}_0|$ can be smaller than $|\mathbf{L}_B|$, which can lead to surprisingly short time intervals between the first and the second GW merger, as explained further in Section 3.2.

and $b' = (b/a_0)(v_\infty/v_c)$, where v_c is here the binary-single characteristic velocity and v_∞ is the relative velocity between the binary and single at infinity (Hut & Bahcall 1983). In this notation $\gamma = 0$ corresponds to a co-planar interaction, and $v_\infty/v_c < 1$ is what is referred to as the HB limit.

The orbit averaged inspiral time of the [BH₁, BH₂] binary, equivalent to the time span t_{12} , can at quadrupole order in the high eccentricity limit be written as (Peters 1964),

$$t_{12} \approx \frac{c^5}{G^3} \frac{4\sqrt{2}}{85} \frac{r_{12}^{7/2} a_{12}^{1/2}}{m_{\text{BH}}^3}. \quad (5)$$

In the limit where the approximations employed in Equation (3) and (4) are valid, the time span t_{12} from Equation (5) can now then be expressed as,

$$t_{12} \approx \frac{\xi a_0^4}{m_{\text{BH}}^3} \left(\frac{a_{12}}{a_0} \right)^{1/2} \frac{|\mathbf{L}_0 + \mathbf{L}_K|^7}{|\mathbf{L}_B|^7}, \quad (6)$$

where we have introduced the following constant,

$$\xi = \frac{c^5}{G^3} \frac{4\sqrt{2}}{85} \left(\frac{3}{16} \right)^{7/2}. \quad (7)$$

For comparison, we note that the inspiral time of the initial circular binary, denoted t_0 , can be written as (Peters 1964),

$$t_0 \approx \frac{\xi a_0^4}{m_{\text{BH}}^3} \frac{1700\sqrt{6}}{81} \approx 2 \cdot 10^5 \text{ yrs} \left(\frac{a_0}{10^{-2} \text{ AU}} \right)^4 \left(\frac{m_{\text{BH}}}{20M_\odot} \right)^{-3}. \quad (8)$$

As seen, the normalizations of t_{12} and t_0 are of similar order (small variations of \mathbf{L}_K easily result in variations of order the

factor of difference $1700\sqrt{6}/81 \approx 51$), which shows the importance of reducing the angular momentum $|\mathbf{L}_0|$ for bringing the time span t_{12} within either the observation time (10^0 – 10^1 years), or the binary-single encounter time (10^7 – 10^8 years).

The relation shown in Equation (6) likewise illustrates that t_{12} will not be significantly affected by GW velocity kicks if $|\mathbf{L}_K| \ll |\mathbf{L}_B|$, which approximately corresponds to the requirement $v_K \ll v_0$, where v_0 denotes the orbital velocity of the initial target binary given by,

$$v_0 \approx 1883 \text{ km s}^{-1} \left(\frac{a_0}{10^{-2} \text{ AU}} \right)^{-1/2} \left(\frac{m_{\text{BH}}}{20M_\odot} \right)^{1/2}. \quad (9)$$

A GW kick of order say 100 km s^{-1} , is therefore not expected to impact the results significantly for the employed normalizations. However, for interactions with a wider initial binary and lower BH masses, moderate GW kicks can easily unbind the system after which a double GW merger is not forming.

Finally, we do note that binary-single systems with a relative high initial angular momentum ($|\mathbf{L}_0| \gtrsim |\mathbf{L}_B|$) can, under rare circumstances, still undergo a prompt double GW merger, provided the GW kick velocity vector is fine-tuned in such a way that $|\mathbf{L}_0 + \mathbf{L}_K| \ll |\mathbf{L}_B|$. Such situations show up in the endstate topology map shown in Figure 2, by a ‘blurring’ of the horizontal edges between the red and the yellow points. In Section 3.3.2 we explore the effect from GW kicks using full numerical simulations.

3.3 Observation of the First and Second GW Merger

We now explore the possibilities for observing both the first and the second GW merger in our proposed double GW merger scenario. For this, we systematically study below how the time span t_{12} depends on the binary-single ICs, and the GW velocity kick from the first merger. The ICs for observing only the second GW merger, i.e. the 2G merger, will be discussed separately in Section 3.4. Our considered cases are described in the paragraphs below.

3.3.1 Interactions with $\gamma = 0$, $v_K = 0$

We start by considering the scenario for which the binary-single interaction is co-planar ($\gamma = 0$), and the GW velocity kick is negligible ($v_K = 0$). This represents an idealized scenario; however, regarding the assumption of $\gamma = 0$, it has been argued that BBHs in disk environments will have their relative orbital inclinations reduced leading to preferentially co-planar interactions (Leigh et al. 2018). Properties of this limit is described in the following.

First, the time span t_{12} can be written by the use of Equation (4) and (6) as,

$$t_{12} \approx \frac{\xi a_0^4}{m_{\text{BH}}^3} \left(\frac{a_{12}}{a_0} \right)^{1/2} \left[1 + \frac{2}{\sqrt{3}} b' \right]^7. \quad (10)$$

From this we see that if the incoming single encounters the initial binary with an impact parameter $b' = b'_0$, where $b'_0 = -\sqrt{3}/2 \approx -0.87$, then the time span $t_{12} \approx 0$, implying the second GW merger happens when BH₁ and BH₂ pass through their first pericenter passage. In this case, the second GW merger will be that of a near head-on BH collision

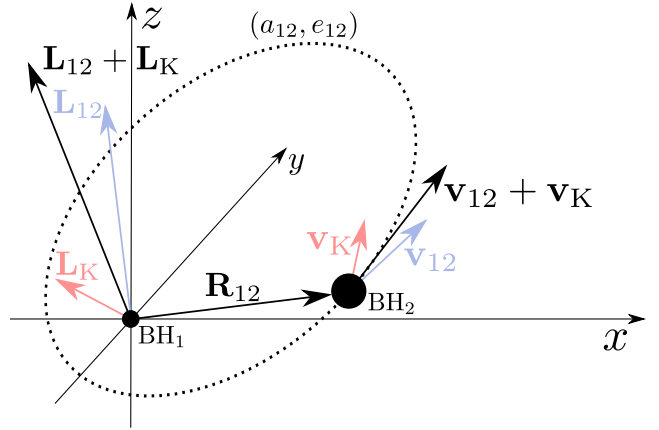


Figure 4. Illustration of the orbital configuration right after the first GW merger. As described in Section 3.1, the first GW merger happens through a two-body GW capture, while the three BHs are still bound to each other. The BH formed as a result of this first GW merger is labeled above by ‘BH₂’, and the remaining single by ‘BH₁’. The relative position vector pointing from BH₁ to BH₂ is labeled by \mathbf{R}_{12} . In the frame of BH₁, BH₂ will right after its formation move with a velocity that is composed of the COM velocity of the two BHs that merged to form BH₂, and the GW kick velocity gained in the GW merger. The COM velocity is labeled by \mathbf{v}_{12} (light blue), the GW kick velocity by \mathbf{v}_K (light red), and the corresponding angular momentum vectors by \mathbf{L}_{12} (light blue) and \mathbf{L}_K (light red), respectively. Right after the first GW merger, BH₂ therefore moves with a velocity $\mathbf{v}_{12} + \mathbf{v}_K$ (solid black) on an orbit with corresponding angular momentum $\mathbf{L}_{12} + \mathbf{L}_K$ (solid black). The SMA and eccentricity of this orbit (black dotted line) is labeled by a_{12}, e_{12} , respectively. If the GW kick velocity is not unbinding the system, then BH₁ and BH₂ will undergo a GW inspiral on a timescale t_{12} that is set by the orbital parameters a_{12}, e_{12} . If t_{12} is short, then both the first and the second GW merger can be observed.

(e.g. Healy et al. 2016). We note here that b'_0 is simply the impact parameter for which the angular momentum of the incoming single exactly cancels the angular momentum of the initial binary (Samsing & Ilan 2018).

In general, double GW mergers can form from interactions with impact parameters in the range $-2 \lesssim b' \lesssim 3$, as seen by the distribution of yellow points in Figure 2. This correspondingly implies that the distribution of t_{12} generally varies over several orders of magnitude, e.g., from Equation (10) we see that $t_{12}(b' = 1)/t_{12}(b' = -1) \approx 10^8$. To gain insight into for which values of b' the second GW merger happens within a timespan of observable interest, we now rewrite Equation (10) as,

$$\Delta b' \approx 0.38 \left(\frac{a_0}{10^{-2} \text{ AU}} \right)^{-4/7} \left(\frac{m_{\text{BH}}}{20M_\odot} \right)^{3/7} \left(\frac{t_{12}}{10 \text{ yrs}} \right)^{1/7}, \quad (11)$$

where we have defined $\Delta b' = |b' - b'_0|$, and omitted the factor with (a_{12}/a_0) , as its power of $-1/14$ makes it unimportant for these estimates. For the employed normalizations, one reads from Equation (11) that all interactions with $b' = b'_0 \pm 0.38$ that result in a double GW merger will have a time span from first to second GW merger $t_{12} < 10$ years. This is interesting as this is not a negligible part of the available phase space; as seen on Figure 2, the range $b'_0 \pm 0.38$ covers about 30% of the relevant f, b' phase space for retrograde interactions ($b' < 0$). We note here that both the position and the

width of the band of red points in Figure 2 are accurately given by -0.87 ± 0.38 . This excellent agreement between our analytical derivations and our 2.5PN numerical N -body simulations, strongly validates our approach and results so far.

We now turn to the question of what the prospects are for observing both GW mergers. For this, we performed a set of numerical binary-single interactions using our 2.5PN N -body code for $\gamma = 0$, $v_K = 0$, and $m_{\text{BH}} = 20M_\odot$, assuming the sampling of b' to be isotropic at infinity. Results are presented in Figure 5, where the black lines show the probability for that a GW merger with eccentricity $e_1 > 0.1$ at 50 Hz (first GW merger) will be followed by a second GW merger within a time span $t_{12} < 10$ years (second GW merger) through the double GW merger scenario, as a function of the initial binary SMA a_0 . This probability we denote by P_{12} to shorten the notations. We note here that prograde interactions ($b' > 0$) will never result in short double GW mergers as this implies that $|\mathbf{L}_0| > |\mathbf{L}_B|$ and thereby $t_{12} \gtrsim t_0$. From the results shown in Figure 5, one concludes that for the ICs considered in this section, the probability for that a GW merger with notable eccentricity in the LIGO band ($e_1 > 0.1$ at 50 Hz) to have a second GW merger within 10 years, is $\gtrsim 0.1$ for $a_0 < 0.1$ AU ($t_0 \lesssim 10^{10}$ years). We note here that ~ 0.1 AU represents roughly the minimum value for a_0 one would find in a classical globular cluster system; below this value the BBH would either have merged before the next encounter, or more likely been dynamically ejected.

To gain insight into how the numerically estimated probability P_{12} shown in Figure 5 changes with the ICs, we can use our analytical expression for $\Delta b'$ from Equation (11). For this, we assume that the f, b' combinations for which $e_1 > 0.1$ at 50 Hz leading to a second GW merger are uniformly distributed near b'_0 , and do not change their large scale topology when the ICs are varied. The latter assumption generally holds, as the large scale topology results from the Newtonian ‘scale-free’ part of the dynamics (Samsing & Ilan 2018). Following this approximation, the probability P_{12} is simply proportional to $\Delta b'$. Using our N -body simulations to calibrate the normalization, one now finds that the probability for a GW merger with eccentricity $e_1 > 0.1$ at 50 Hz to be followed by a second GW merger within time span $t_{12} < \tau$ years, has the following analytical solution,

$$P_{12} \approx 0.26 \left(\frac{a_0}{10^{-2} \text{AU}} \right)^{-4/7} \left(\frac{m_{\text{BH}}}{20M_\odot} \right)^{3/7} \left(\frac{\tau}{10 \text{ yrs}} \right)^{1/7}, \quad (12)$$

where the factor (a_{12}/a_0) again has been omitted. Although the assumption of a uniform distribution breaks down in a few regions near b'_0 (See Figure 2), we do find that our analytical solution from the above Equation (12) fits our numerical results quite well. As an illustrative example, the scaling with a_0 is shown in Figure 5 by the *black dotted line*. From comparing with Figure 2, the deviation from a pure powerlaw at low a_0 is indeed due to that the assumption of a uniform distribution breaks down when $\Delta b'$ becomes to large, or equivalently when a_0 becomes to small. We further note that P_{12} in Equation (12) depends very weakly on τ , which implies that the results shown in Figure 5 are not sensitive to the exact value of the time span limit τ . Below we study the role of GW kicks in this co-planar scenario.

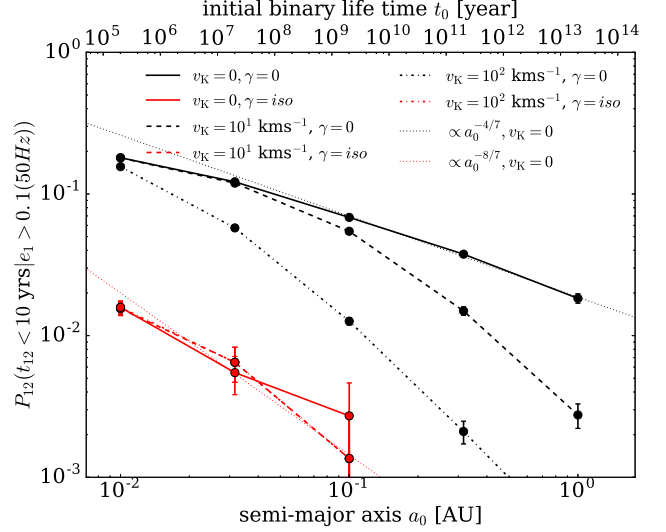


Figure 5. Probability, P_{12} , that a BBH merger with eccentricity $e_1 > 0.1$ at 50 Hz (first GW merger) is followed by a GW merger (second GW merger) within a time span of $t_{12} < 10$ years through our proposed double GW merger scenario. The mass of the BHs are $m_{\text{BH}} = 20M_\odot$, and the probability is shown as a function of the SMA of the initial target binary, a_0 . The *solid*, *dashed*, and *dash-dotted* lines show P_{12} derived from full numerical binary-single simulations, for when the BH formed in the first GW merger, BH_2 , receives a GW velocity kick of 0 km s^{-1} , 10 km s^{-1} , and 100 km s^{-1} , respectively. For initial spinning BHs v_K can easily reach values of 1000 km s^{-1} , which will lead to prompt disruption and no second GW merger. For these simulations, we have assumed that the pointing of the GW kick velocity vector \mathbf{v}_K is isotropic, and the mass of BH_2 is $2m_{\text{BH}}$. The *black lines* show results from co-planar interactions ($\gamma = 0$), where the *red lines* show results from isotropic interactions ($\gamma = \text{iso}$). The *dotted lines* show analytical scaling relations valid in the $v_K = 0$ limit. The *top axis* shows the GW inspiral life time of the initial circular binary in years. As seen, it is highly unlikely that isotropic environments, such as classical globular clusters, will result in observable double GW mergers. However, co-planar interactions do generally lead to much shorter merger time scales, which correspondingly lead to a measurable fraction of double GW mergers.

3.3.2 Interactions with $\gamma = 0$, $v_K > 0$

Binary-single interactions with $\gamma \approx 0$ and $v_K = 0$ represent the optimal scenario for producing double GW mergers with short enough time span t_{12} to be observed. However, GW kicks are expected, so here we explore how the inclusion of GW velocity kicks affects this case, by focusing on how the fraction of double GW mergers with $t_{12} < 10$ years changes with varying v_K . For this, we use our N -body code to numerically calculate the probability P_{12} , shown in Figure 5, for when the BH formed in the first GW merger, BH_2 , receives a velocity kick v_K of either 10 km s^{-1} or 100 km s^{-1} at its formation.

Results for varying v_K are shown in Figure 5. As seen in the figure, GW kicks significantly reduces the fraction of double GW mergers with $t_{12} < 10$ years, especially for binaries with $a_0 > 0.1$ AU. Binaries with $a_0 < 0.1$ AU are less affected, as their orbital velocity is much higher; however, they are at the same time less likely to exist, as they initially have a very short life time as indicated by the up-

per x-axis. Depending on the exact properties of their host stellar system, very hard binaries are in fact likely to merge in-between encounters (e.g. Samsing 2017). Although GW kicks are expected, we do note that several recent studies have in fact looked into the observational consequences of BHs forming with near zero spin, which generally also leads to low kicks (e.g. Rodriguez et al. 2018). This limit allows for the formation of second-generation GW mergers, which are characterized by mass ratios of about 1 : 2 and relative high BH spins around 0.7. In the section below we extend our analysis from this section to varying γ , including the isotropic case found in globular clusters.

3.3.3 Interactions with $\gamma > 0$, $v_K \geq 0$

We now study how varying the orbital inclination angle γ and kick velocity v_K affect the time span t_{12} . This is done to explore the role and formation probability of double GW mergers in classical stellar systems, such as globular clusters.

To gain insight into how a varying γ changes the picture described in Section 3.3.1 and 3.3.2, we first consider what the minimum value for t_{12} is as a function of γ , assuming the optimal case for which $v_K = 0$. By minimizing the expression for t_{12} given by Equation (6) w.r.t. b' for fixed value of γ , we find that the minimum value of t_{12} , denoted here by $\min(t_{12})$, can be written as,

$$\min(t_{12}) \approx \frac{\xi a_0^4}{m_{\text{BH}}^3} \left(\frac{a_{12}}{a_0} \right)^{1/2} \sin^7(\gamma), \quad (13)$$

where the corresponding $b'(\min(t_{12}))$ equals $-\cos(\gamma)\sqrt{3}/2$. We here see that the formation of prompt double GW mergers with $\min(t_{12}) \approx 0$ is only possible in the special case for which $\gamma = 0$. Considering the limit where $\sin(\gamma) \approx \gamma$, we can rewrite the above Equation (13) in the following form,

$$\gamma \approx 20^\circ \left(\frac{a_0}{10^{-2} \text{AU}} \right)^{-4/7} \left(\frac{m_{\text{BH}}}{20 M_\odot} \right)^{3/7} \left(\frac{\min(t_{12})}{10 \text{ yrs}} \right)^{1/7}, \quad (14)$$

where the factor (a_{12}/a_0) again has been omitted. This relation tells us that for $a_0 = 10^{-2}(10^{-1})$ AU interactions with $\gamma > 20^\circ(5^\circ)$ will not be able to result in a double GW merger with a timespan $t_{12} < 10$ years. Observable double GW mergers are therefore most likely to form in near co-planar interactions.

To study what the actual fraction of observable double GW mergers is in the isotropic case, and how much smaller it is compared to the co-planar case, we performed $\sim 10^6$ 2.5PN numerical scatterings assuming an isotropic binary-single encounter distribution. Results are shown in Figure 5 with red lines. As seen, the fraction is greatly reduced, which originates from the fact that most of the phase space ($\gamma > \mathcal{O}(10^\circ)$) sampled in the isotropic case leads to a time span t_{12} far too long for both mergers to be observed. As a result, in terms of rates, isotropic environments, such as a globular cluster, are not likely to significantly contribute to the formation of observable double GW mergers.

The probability P_{12} also scales differently with a_0, m_{BH} and τ than found in the co-planar case. The differences relate to the difference in eccentricity distributions (e.g. Valtonen & Karttunen 2006; Leigh et al. 2018); in the isotropic case eccentricity tends to follow a thermal distribution $2e$, whereas in the co-planar case the distri-

bution can be shown to instead follow $e/\sqrt{1-e^2}$ (e.g. Valtonen & Karttunen 2006). Assuming e_{12} follow these distributions in the two scenarios, one finds in the isotropic case that $P_{12} \propto a_0^{-8/7} m_{\text{BH}}^{6/7} \tau^{2/7}$ and in the co-planar case $P_{12} \propto a_0^{-4/7} m_{\text{BH}}^{3/7} \tau^{1/7}$ (in agreement with Equation 12). That P_{12} falls off steeper with a_0 in the isotropic case than the co-planar case, also provides some insight into why the fraction of double GW mergers from isotropic scatterings is vanishing for classical system for which $a_0 > 0.1$ AU. The prospects of detecting prompt 2G mergers is described in the section below.

3.4 Observation of the Second Merger

Having argued that *directly* observing both the first and the second GW merger is only possible in near co-planar interactions and unlikely for isotropic environments, we now turn to the question if our proposed double GW merger scenario instead can be *indirectly* observed. With indirect we here refer to the case where only the prompt 2G merger is seen. As explained earlier, such a merger would be characterized by a mass ratio of about 1 : 2 and (at least) one BH highly spinning (e.g. Rodriguez et al. 2018). For this scenario to take place, the GW life time of the second GW merger must be shorter than the typical time between binary-single encounters, which depends on the number density of single BHs, n_s , and the velocity dispersion, v_{disp} , of the dynamical environment as $(n_s \sigma_{\text{bs}} v_{\text{disp}})^{-1}$, where σ_{bs} is the binary-single interaction cross section (see e.g. Samsing 2017; Samsing et al. 2018). In the following we discuss the prospects for observing this second GW merger, i.e. the prompt 2G merger, in a typical globular cluster system in which the time between encounters is $< 10^8$ years.

Numerical scattering results are presented in Figure 6, which shows the probability for that the second GW merger occurs within 10^8 years, for a BBH with an initial SMA $a_0 = 10^{-0.5} \approx 0.3$ AU and $m_{\text{BH}} = 20 M_\odot$, as a function of the GW kick velocity, v_K . The black line shows the co-planar case, where the red line shows the isotropic case. From considering the normalization of the isotropic case, we conclude that only $\sim 2\%$ of all BBH mergers that form during three-body interactions will also undergo a second GW merger before the next encounter disrupts the system. From this we draw the following two conclusions.

First, the $[\text{BH}_1, \text{BH}_2]$ binary formed after the first GW merger is more likely to undergo a subsequent binary-single interaction, than ending as a prompt 2G merger. The reason is simply that the typical time span from the first to the second GW merger, t_{12} , is in the majority of cases much longer than the characteristic time between encounters. The binary $[\text{BH}_1, \text{BH}_2]$ formed after the first GW merger will therefore most often keep interacting and thereby contribute dynamically to the evolution of the stellar system. We note that this is not necessarily the case for BHs formed in 2G mergers, as the most likely outcome here is ejection as the $[\text{BH}_1, \text{BH}_2]$ binary will be of unequal mass with one of the BHs (highly) spinning at about 0.7; combinations that are expected to generate large GW kicks. A buildup and dynamical influence of third-generation BHs is therefore both difficult and unlikely.

Second, if GW mergers are observed with a notable

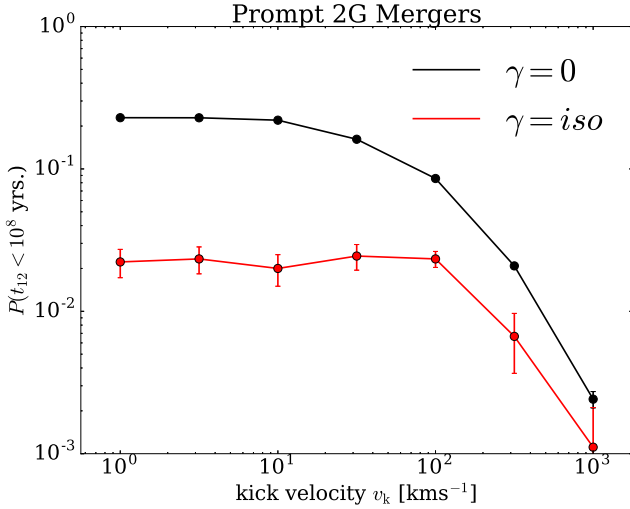


Figure 6. The probability that a binary-single interaction that first undergoes a GW merger during the interaction (first GW merger) subsequently undergoes one more GW merger (second GW merger) within a typical encounter time scale of the host stellar system. In this figure, this time scale is set to 10^8 years. The probability is derived for a BBH with initial SMA $a_0 = 10^{-0.5}$ AU and $m_{\text{BH}} = 20M_{\odot}$, as a function of the GW kick velocity, v_k . The *black line* shows results from co-planar interactions ($\gamma = 0$), where the *red line* shows from isotropic interactions ($\gamma = iso$). As seen, only a few percent of the three-body systems that first undergo a GW merger during the interaction will undergo a second GW merger before interacting with a new single BH. Observations of second-generation BBH mergers forming in isotropic systems, are therefore not expected to be dominated by the double GW merger scenario. On the other hand, a notable fraction of all co-planar interactions will undergo both the first and the second GW merger. Such ICs also give rise to very short merger time spans t_{12} as seen in Figure 5. It is currently unclear if co-planar environments exist, although they have been suggested in the recent literature (e.g. Leigh et al. 2018).

mass ratio about 1 : 2 and one BH with spin ~ 0.7 , then the most likely origin is a second-generation merger formed after the BH assembled in the first merger has swapped partner at least once, i.e., it is less likely that the merger was produced in the double GW merger scenario. As described earlier, second generation BBH mergers form either doing or in-between binary-single interactions (e.g. Samsing 2017; Rodriguez et al. 2018). Subsequent interactions also allow for the possibility that two second-generation BHs meet each other and merge, leading to relative heavy equal mass binaries. Such scenarios have recently been explored by e.g. Gerosa & Berti (2017); Rodriguez et al. (2018), and would point towards a dynamical origin. We conclude our study in the section below.

4 CONCLUSIONS

We have in this paper presented a study on BH binary-single interactions resulting in two successive GW mergers, an outcome we refer to as a double GW merger. Double GW mergers are a natural outcome when GR effects are included in the N -body EOM (Samsing & Ilan 2018), but several mechanisms can prevent them from happen, such as GW

kicks. The formation of double GW mergers have been proposed and presented in the past literature both numerically (Campanelli et al. 2008) and dynamically (Samsing & Ilan 2018); however, our presented study is the first to quantify their actual formation probability and in which environments they are most likely to form. Double GW mergers are interesting as they give rise to unique observables, which could help distinguishing between BBH merger channels. A brief summary of our findings is given below.

The double GW merger scenario produces at least two unique observable signatures that are different from other formation channels, especially the class that does not involve few-body dynamics.

The first signature, is the observation of both the first and the second GW merger in the scenario. This requires the time span between the two mergers to be short ($t_{12} < O(\text{years})$), which is orders of magnitude shorter than the initial target binary life time. Using numerical and analytical arguments we have shown that only interactions that are near co-planar will be able to produce such short double GW mergers. The reason is that in near co-planar systems the angular momentum carried by the incoming single can lead to a near cancellation of the initial BBH angular momentum, which correspondingly leads to a very short merger time scale (e.g. Samsing & Ilan 2018). In the case where the encounters are instead isotropic, the overall probability for forming an observable double GW merger decreases drastically (Figure 5), as the majority of the available phase space (away from near co-planar configurations) will lead to merger times that are far too long. From this we conclude that if both mergers in the scenario are observed, then this would be an indirect probe of environments facilitating co-planar interactions; this includes in particular disk systems, such as active galactic nuclei (e.g. Leigh et al. 2018).

The second signature, is the observation of only the second GW merger, that we refer to as a prompt 2G merger. As pointed out in Gerosa & Berti (2017); Rodriguez et al. (2018), second-generation BBH mergers are generally characterized by a mass ratio of about 1 : 2, and at least one highly spinning BH. Using numerical scatterings we have shown that the probability for a binary-single interaction to undergo an observable 2G merger in the isotropic case, is still only at the percent level. Second-generation GW mergers can form in other ways than through our proposed double GW merger scenario (e.g. Gerosa & Berti 2017; Samsing 2017; Rodriguez et al. 2018), and such mergers are therefore not expected to be a unique signature of the double GW merger scenario, although they still indicate that dynamical environments are able to produce BBH mergers.

To conclude, the formation of double GW mergers have been suggested in the past literature, and their unique observables have been numerically studied (e.g. Campanelli et al. 2008). We have studied their formation probability, and found that they are not expected to form in measurable numbers in classical isotropic stellar systems, such as globular clusters. A significant fraction can only form in near co-planar environments, which could be active galactic nuclei disks (e.g. Bartos et al. 2017; Stone et al. 2017; McKernan et al. 2017; Leigh et al. 2018). This makes it currently impossible to predict reliable rates, as such disk systems at present are still poorly understood. Hopefully our study motivates the community to look into this further.

ACKNOWLEDGEMENTS

Support for this work was provided by NASA through Einstein Postdoctoral Fellowship grant number PF4-150127 awarded by the Chandra X-ray Center, which is operated by the Smithsonian Astrophysical Observatory for NASA under contract NAS8-03060. TI thanks the Undergraduate Summer Research Program (USRP) at the department of Astrophysical Sciences, Princeton University, for support. JS thanks the Niels Bohr Institute for its hospitality while part of this work was completed, and the Kavli Foundation and the DNRf for supporting the 2017 Kavli Summer Program.

REFERENCES

- Abbott B. P., et al., 2016a, *Physical Review X*, **6**, 041015
 Abbott B. P., et al., 2016b, *Physical Review Letters*, **116**, 061102
 Abbott B. P., et al., 2016c, *Physical Review Letters*, **116**, 241103
 Abbott B. P., et al., 2016d, *ApJ*, **818**, L22
 Abbott B. P., et al., 2017a, *Physical Review Letters*, **118**, 221101
 Abbott B. P., et al., 2017b, *Physical Review Letters*, **119**, 141101
 Antonini F., Rasio F. A., 2016, *ApJ*, **831**, 187
 Antonini F., Chatterjee S., Rodriguez C. L., Morscher M., Pattabiraman B., Kalogera V., Rasio F. A., 2016, *ApJ*, **816**, 65
 Askar A., Szkudlarek M., Gondek-Rosińska D., Giersz M., Bulik T., 2017, *MNRAS*, **464**, L36
 Bae Y.-B., Kim C., Lee H. M., 2014, *MNRAS*, **440**, 2714
 Bae Y.-B., Lee H. M., Kang G., Hansen J., 2017, preprint, ([arXiv:1701.01548](https://arxiv.org/abs/1701.01548))
 Baker J. G., Centrella J., Choi D.-I., Koppitz M., van Meter J. R., Miller M. C., 2006, *ApJ*, **653**, L93
 Banerjee S., Baumgardt H., Kroupa P., 2010, *MNRAS*, **402**, 371
 Bartos I., Kocsis B., Haiman Z., Márka S., 2017, *ApJ*, **835**, 165
 Belczynski K., Holz D. E., Bulik T., O’Shaughnessy R., 2016a, *Nature*, **534**, 512
 Belczynski K., Repetto S., Holz D. E., O’Shaughnessy R., Bulik T., Berti E., Fryer C., Dominik M., 2016b, *ApJ*, **819**, 108
 Bellovary J. M., Mac Low M.-M., McKernan B., Ford K. E. S., 2016, *ApJ*, **819**, L17
 Bird S., Cholis I., Muñoz J. B., Ali-Haïmoud Y., Kamionkowski M., Kovetz E. D., Raccanelli A., Riess A. G., 2016, *Physical Review Letters*, **116**, 201301
 Blanchet L., 2006, *Living Reviews in Relativity*, **9**
 Campanelli M., Lousto C. O., Zlochower Y., 2008, *Phys. Rev. D*, **77**, 101501
 Carr B., Kühnel F., Sandstad M., 2016, *Phys. Rev. D*, **94**, 083504
 Centrella J., Baker J. G., Kelly B. J., van Meter J. R., 2010, *Reviews of Modern Physics*, **82**, 3069
 Cholis I., Kovetz E. D., Ali-Haïmoud Y., Bird S., Kamionkowski M., Muñoz J. B., Raccanelli A., 2016, *Phys. Rev. D*, **94**, 084013
 Dominik M., Belczynski K., Fryer C., Holz D. E., Berti E., Bulik T., Mandel I., O’Shaughnessy R., 2012, *ApJ*, **759**, 52
 Dominik M., Belczynski K., Fryer C., Holz D. E., Berti E., Bulik T., Mandel I., O’Shaughnessy R., 2013, *ApJ*, **779**, 72
 Dominik M., et al., 2015, *ApJ*, **806**, 263
 Farr W. M., Stevenson S., Miller M. C., Mandel I., Farr B., Vecchio A., 2017, preprint, ([arXiv:1706.01385](https://arxiv.org/abs/1706.01385))
 Fregeau J. M., Cheung P., Portegies Zwart S. F., Rasio F. A., 2004, *MNRAS*, **352**, 1
 Gerosa D., Berti E., 2017, *Phys. Rev. D*, **95**, 124046
 Gondán L., Kocsis B., Raffai P., Frei Z., 2017, preprint, ([arXiv:1705.10781](https://arxiv.org/abs/1705.10781))
 González J. A., Spherhake U., Brüggemann B., Hannam M., Husa S., 2007, *Physical Review Letters*, **98**, 091101
 Gültekin K., Miller M. C., Hamilton D. P., 2006, *ApJ*, **640**, 156
 Hansen R., 1972, *Phys. Rev. D*, **5**, 1021
 Harry I., Privitera S., Bohé A., Buonanno A., 2016, *Phys. Rev. D*, **94**, 024012
 Healy J., Ruchlin I., Lousto C. O., Zlochower Y., 2016, *Phys. Rev. D*, **94**, 104020
 Hoggie D. C., 1975, *MNRAS*, **173**, 729
 Hoang B.-M., Naoz S., Kocsis B., Rasio F. A., Dosopoulou F., 2017, preprint, ([arXiv:1706.09896](https://arxiv.org/abs/1706.09896))
 Hong J., Lee H. M., 2015, *MNRAS*, **448**, 754
 Huerta E. A., et al., 2017, *Phys. Rev. D*, **95**, 024038
 Huerta E. A., et al., 2018, *Phys. Rev. D*, **97**, 024031
 Hut P., 1983a, *AJ*, **88**, 1549
 Hut P., 1983b, *ApJ*, **268**, 342
 Hut P., 1993, *ApJ*, **403**, 256
 Hut P., Bahcall J. N., 1983, *ApJ*, **268**, 319
 Kalogera V., 2000, *ApJ*, **541**, 319
 Kocsis B., Tremaine S., 2011, *MNRAS*, **412**, 187
 Kocsis B., Tremaine S., 2015, *MNRAS*, **448**, 3265
 Lehner L., Pretorius F., 2014, *ARA&A*, **52**, 661
 Leigh N. W. C., et al., 2018, *MNRAS*, **474**, 5672
 McKernan B., et al., 2017, preprint, ([arXiv:1702.07818](https://arxiv.org/abs/1702.07818))
 O’Leary R. M., Kocsis B., Loeb A., 2009, *MNRAS*, **395**, 2127
 Park D., Kim C., Lee H. M., Bae Y.-B., Belczynski K., 2017, *MNRAS*, **469**, 4665
 Peters P., 1964, *Phys. Rev.*, **136**, B1224
 Portegies Zwart S. F., McMillan S. L. W., 2000, *ApJ*, **528**, L17
 Rodriguez C. L., Antonini F., 2018, preprint, ([arXiv:1805.08212](https://arxiv.org/abs/1805.08212))
 Rodriguez C. L., Morscher M., Pattabiraman B., Chatterjee S., Haster C.-J., Rasio F. A., 2015, *Physical Review Letters*, **115**, 051101
 Rodriguez C. L., Chatterjee S., Rasio F. A., 2016a, *Phys. Rev. D*, **93**, 084029
 Rodriguez C. L., Haster C.-J., Chatterjee S., Kalogera V., Rasio F. A., 2016b, *ApJ*, **824**, L8
 Rodriguez C. L., Zevin M., Pankow C., Kalogera V., Rasio F. A., 2016c, *ApJ*, **832**, L2
 Rodriguez C. L., Amaro-Seoane P., Chatterjee S., Rasio F. A., 2018, *Physical Review Letters*, **120**, 151101
 Roupas Z., Kocsis B., Tremaine S., 2017, *ApJ*, **842**, 90
 Samsing J., 2017, preprint, ([arXiv:1711.07452](https://arxiv.org/abs/1711.07452))
 Samsing J., Ilan T., 2018, *MNRAS*, **476**, 1548
 Samsing J., Ramirez-Ruiz E., 2017, *ApJ*, **840**, L14
 Samsing J., MacLeod M., Ramirez-Ruiz E., 2014, *ApJ*, **784**, 71
 Samsing J., MacLeod M., Ramirez-Ruiz E., 2017, *ApJ*, **846**, 36
 Samsing J., MacLeod M., Ramirez-Ruiz E., 2018, *ApJ*, **853**, 140
 Sasaki M., Suyama T., Tanaka T., Yokoyama S., 2016, *Physical Review Letters*, **117**, 061101
 Silsbee K., Tremaine S., 2017, *ApJ*, **836**, 39
 Stone N. C., Metzger B. D., Haiman Z., 2017, *MNRAS*, **464**, 946
 Tanikawa A., 2013, *MNRAS*, **435**, 1358
 Valtonen M., Karttunen H., 2006, *The Three-Body Problem*
 VanLandingham J. H., Miller M. C., Hamilton D. P., Richardson D. C., 2016, *ApJ*, **828**, 77
 Voss R., Tauris T. M., 2003, *MNRAS*, **342**, 1169
 Wen L., 2003, *ApJ*, **598**, 419
 Zevin M., Pankow C., Rodriguez C. L., Sampson L., Chase E., Kalogera V., Rasio F. A., 2017, *ApJ*, **846**, 82

This paper has been typeset from a $\text{\TeX}/\text{\LaTeX}$ file prepared by the author.